Multibody Syst Dyn (2017) 39:79–94
DOI 10.1007/s11044-016-9533-8

A maximal monotone impact law for the 3-ball Newton's cradle

Tom Winandy[1] · **Remco I. Leine**[1]

Received: 5 November 2015 / Accepted: 13 August 2016 / Published online: 31 August 2016

Abstract The 3-ball Newton's cradle is used as a stepping stone to divulge the structure of impact laws. A continuous conewise linear impact law that maps the preimpact contact velocities to the postimpact contact velocities is proposed for the 3-ball Newton's cradle. The proposed impact law is kinematically, kinetically, and energetically consistent. It reproduces the outcomes of experimental observation. Moreover, it is in accordance with the outcome of the collision of three identical linear-elastic thin rods for which the impact process is governed by the one-dimensional wave equation. The proposed impact law is shown to be nonexpansive. Therefore, the relationship between the mean contact velocity and its dual, the impulsive force, is maximal monotone. A counterexample to maximal cyclical monotonicity of this relationship allows us to conclude that no dissipation function exists for the proposed impact law.

Keywords Newton's cradle · Unilateral constraints · Impact · Convex analysis · Wave equation

1 Introduction

In this paper, we present an instantaneous impact law for Newton's cradle with three balls. We construct a continuous cone-wise linear impact law which is energy conserving and provides the classical outcomes of the 3-ball Newton's cradle [22]. The outcomes of the proposed instantaneous impact law are in accordance with the results of the elastic rod model, which is governed by the one-dimensional wave equation.

Rigid multibody dynamics has currently two instantaneous impact laws for multicollisions at its disposal, the generalized Newton's impact law and the generalized Poisson's

✉ T. Winandy
winandy@inm.uni-stuttgart.de

R.I. Leine
leine@inm.uni-stuttgart.de

[1] Institute for Nonlinear Mechanics, University of Stuttgart, Pfaffenwaldring 9, 70569 Stuttgart, Germany

impact law [2, 4, 6–8, 14]. Both laws agree for inelastic collisions and are in accordance with experimental results if wave phenomena are absent. The laws give different results for partially elastic multicollisions. In very particular cases, when also dry friction is included, Newton's and Poisson's impact laws may lead to an energy increase, contradicting the laws of thermodynamics, even if all restitution coefficients are chosen smaller than unity [7]. In the current paper, the focus is on frictionless completely elastic multicollisions in which wave phenomena are dominant. Thereby, the dissipation that is present in a physical system is neglected in order to focus on the mathematical structure of the impact law.

In order to set the scene of this paper, consider the classical Newton's cradle problem with three balls and assume that there is no dissipation (see Fig. 1). The left ball has velocity v and hits the middle and right balls, which are standing still. Two contacts are closed at the collision time instant. The problem is therefore an archetype of a multicollision [1]. The generalized Newton's and Poisson's impact laws both forecast for this case the same post-impact velocities: the left ball is returning with one third of the velocity, and the middle and right balls are moving with two-third of the velocity to the right. The prediction of the generalized Newton's and Poisson's impact laws respects the balance of linear momentum and the conservation of energy. However, if one performs a tabletop experiment with iron balls and neglects small inner vibration, then one observes that the left and middle balls remain at rest after the impact and the right ball is expelled with velocity v. Currently, rigid multibody dynamics does not possess an instantaneous impact law that describes the observations of Newton's cradle.

The aim of this paper is to find an instantaneous impact law that describes all observations of the 3-ball Newton's cradle and to study the mathematical properties of this impact law, which may divulge a general mathematical structure of a multicollision impact law for completely elastic collisions. The kinematics and kinetics of the 3-ball Newton's cradle is described in Sect. 2, and a number of important properties of impact laws are introduced. In Sect. 3, an impact law is proposed that describes all observations. It is shown in Sect. 4 that a thin elastic rod model agrees with these observations. Section 5 deals with impact models involving compliant contacts. The contraction properties of the proposed impact law are studied in Sect. 6. Conclusions on whether the results of the 3-ball Newton's cradle may be generalized are drawn in Sect. 7.

2 The 3-ball Newton's cradle

The 3-ball Newton's cradle is shown in Fig. 1(a). It consists of three balls of equal mass m with horizontal positions $\mathbf{q} = (q_1 \ q_2 \ q_3)^{\mathrm{T}}$ and velocities $\dot{\mathbf{q}} = \mathbf{u} = (u_1 \ u_2 \ u_3)^{\mathrm{T}}$. The contact distances are given by $\mathbf{g} = (g_1 \ g_2)^{\mathrm{T}} = (q_2 - q_1 - 2R \ \ q_3 - q_2 - 2R)^{\mathrm{T}}$, where R is the radius of the balls. The unilateral constraint $\mathbf{g} \geq \mathbf{0}$ expresses the fact that contacts can open but that the balls may not penetrate each other. In order to illustrate the concept, consider the contact between the left and middle balls. The distance between the balls is given by the gap function g_1 of the contact. For $g_1 = 0$, there is no gap, that is, the contact is closed. For $g_1 > 0$, there is a gap between the balls, which means that the contact is open. Demanding $g_1 \geq 0$ then means that the contact between the left ball and the middle ball can be either open or closed, but that the balls cannot penetrate. The contact velocities are given by the relative velocities between the balls $\boldsymbol{\gamma} = (\gamma_1 \ \gamma_2)^{\mathrm{T}} = (u_2 - u_1 \ u_3 - u_2)^{\mathrm{T}}$, that is, $\boldsymbol{\gamma} = \dot{\mathbf{g}}$ whenever it exists. The pre- and postimpact velocities are designated by $\mathbf{u}^-$ and $\mathbf{u}^+$, respectively. Analogously, $\boldsymbol{\gamma}^-$ and $\boldsymbol{\gamma}^+$ designate the pre- and postimpact contact velocities.

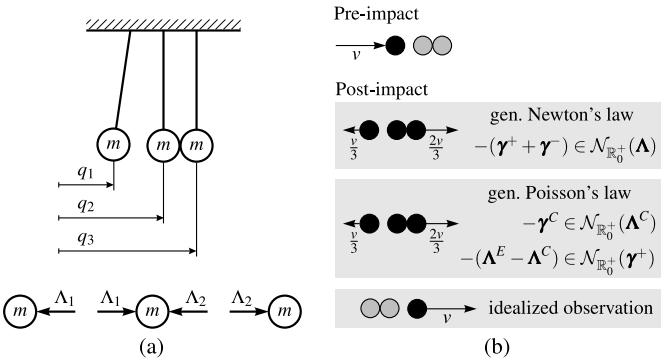

Fig. 1 *Left*: Newton's cradle with three balls of mass m. *Right*: An example of outcomes by Newton's and Poisson's impact laws

The impact equations of the system can be written in the following matrix form:

$$\mathbf{M}\left(\mathbf{u}^{+}-\mathbf{u}^{-}\right)=\mathbf{W}\boldsymbol{\Lambda}, \tag{1}$$

$$\boldsymbol{\gamma}^{\pm}=\mathbf{W}^{\mathrm{T}}\mathbf{u}^{\pm}, \tag{2}$$

where $\boldsymbol{\Lambda}=(\Lambda_1\ \Lambda_2)^{\mathrm{T}}$ are the impulsive contact forces during the impact. The impulsive force Λ_1 acts between balls 1 and 2, whereas Λ_2 occurs between balls 2 and 3. Note that this paper deals with the description of instantaneous impacts. By modeling the impact process as an instantaneous impact the impact process is reduced to a singular instant of time, which is called the time of impact. The impact equation (1) relates the discontinuity of the velocities to the impulsive contact forces at the time of impact. The adjective "impulsive" is used to emphasize the difference to a force. The difference becomes obvious if we compare the units of a contact force λ [N] and an impulsive contact force Λ [Ns].

The combination of (1) and (2) yields the impact equation in contact velocities

$$\boldsymbol{\gamma}^{+}-\boldsymbol{\gamma}^{-}=\mathbf{G}\boldsymbol{\Lambda}\quad\text{with}\quad\mathbf{G}:=\mathbf{W}^{\mathrm{T}}\mathbf{M}^{-1}\mathbf{W}. \tag{3}$$

The matrix $\mathbf{G}$ is referred to as the Delassus operator. The matrix $\mathbf{W}$ is the matrix of generalized force directions for which $\mathbf{W}^{\mathrm{T}}=\frac{\partial\mathbf{g}}{\partial\mathbf{q}}$. For the 3-ball Newton's cradle, the mass matrix $\mathbf{M}$ and the matrix of generalized force directions $\mathbf{W}$ are

$$\mathbf{M}=\begin{pmatrix}m&0&0\\0&m&0\\0&0&m\end{pmatrix}\quad\text{and}\quad\mathbf{W}=\begin{pmatrix}-1&0\\1&-1\\0&1\end{pmatrix}. \tag{4}$$

The impact equation (3) needs to be complemented by an impact law, being a constitutive relationship, which may be expressed by a set-valued relationship between dual variables [13]

$$-\boldsymbol{\Lambda}\in\mathcal{H}(\bar{\boldsymbol{\gamma}}), \tag{5}$$

where

$$\bar{\boldsymbol{\gamma}}=\frac{1}{2}\left(\boldsymbol{\gamma}^{+}+\boldsymbol{\gamma}^{-}\right) \tag{6}$$

is referred to as the mean contact velocity. The operator $\mathcal{H}\colon \mathbb{R}^n \rightrightarrows \mathbb{R}^n$ is in general a set-valued operator.

Alternatively to the formulation as a set-valued relationship (5), the impact law can be expressed by a mapping S from pre- to postimpact contact velocities

$$\boldsymbol{\gamma}^+ = S\left(\boldsymbol{\gamma}^-\right), \tag{7}$$

or by a mapping Z from pre- to postimpact generalized velocities

$$\mathbf{u}^+ = Z\left(\mathbf{u}^-\right). \tag{8}$$

The set-valued operator $\mathcal{H}$ and the single-valued mappings S and Z are all different formulations of the same impact law. Specifying one in closed form directly implies an (implicit) formulation of the other representations.

An impact law should be kinematically, kinetically, and energetically consistent:

– Preimpact contact velocities $\boldsymbol{\gamma}^-$ and postimpact contact velocities $\boldsymbol{\gamma}^+$ are called *kinematically admissible* if

$$\boldsymbol{\gamma}^- \leq \mathbf{0} \quad \text{and} \quad \boldsymbol{\gamma}^+ \geq \mathbf{0}, \tag{9}$$

respectively. An impact law is *kinematically consistent* if it yields kinematically admissible postimpact velocities for arbitrary preimpact velocities.

– *Kinetic consistency* is required by the unilateral character of nonadhesive contacts, which requires the contact forces to be nonnegative:

$$\boldsymbol{\Lambda} \geq \mathbf{0}. \tag{10}$$

The contact force Λ_i of contact i vanishes if the contact is open, that is, if $g_i > 0$. If $g_i = 0$, then contact i is closed and can only transfer nonnegative contact forces.

– *Energetic consistency* means that there is no increase in energy during the impact. Let the kinetic energy before and after the impact be designated by $T^- = \frac{1}{2}\mathbf{u}^{-\mathrm{T}}\mathbf{M}\mathbf{u}^-$ and $T^+ = \frac{1}{2}\mathbf{u}^{+\mathrm{T}}\mathbf{M}\mathbf{u}^+$, respectively. Energetic consistency then requires that

$$T^+ \leq T^- \quad \Leftrightarrow \quad T^+ - T^- \leq 0, \tag{11}$$

which can be expressed in terms of pre- and postimpact velocities by

$$\mathbf{u}^{+\mathrm{T}}\mathbf{M}\mathbf{u}^+ - \mathbf{u}^{-\mathrm{T}}\mathbf{M}\mathbf{u}^- = \left(\mathbf{u}^+ + \mathbf{u}^-\right)^{\mathrm{T}}\mathbf{M}\left(\mathbf{u}^+ - \mathbf{u}^-\right) \leq 0. \tag{12}$$

The use of (1), (2), and (3) permits to rewrite (12) as

$$\left(\boldsymbol{\gamma}^+ + \boldsymbol{\gamma}^-\right)^{\mathrm{T}}\mathbf{G}^{-1}\left(\boldsymbol{\gamma}^+ - \boldsymbol{\gamma}^-\right) = \boldsymbol{\gamma}^{+\mathrm{T}}\mathbf{G}^{-1}\boldsymbol{\gamma}^+ - \boldsymbol{\gamma}^{-\mathrm{T}}\mathbf{G}^{-1}\boldsymbol{\gamma}^- \leq 0. \tag{13}$$

Conditions (12) and (13) for energetic consistency can be expressed using the norms with metrics induced by $\mathbf{M}$ and $\mathbf{G}^{-1}$, respectively, by

$$\left\|\mathbf{u}^+\right\|_{\mathbf{M}}^2 \leq \left\|\mathbf{u}^-\right\|_{\mathbf{M}}^2 \quad \text{and} \quad \left\|\boldsymbol{\gamma}^+\right\|_{\mathbf{G}^{-1}}^2 \leq \left\|\boldsymbol{\gamma}^-\right\|_{\mathbf{G}^{-1}}^2. \tag{14}$$

From [13, 19] it is known that the maximal monotonicity of the operator $\mathcal{H}$ in (5) is equivalent to nonexpansivity properties of the impact mappings (7) and (8).

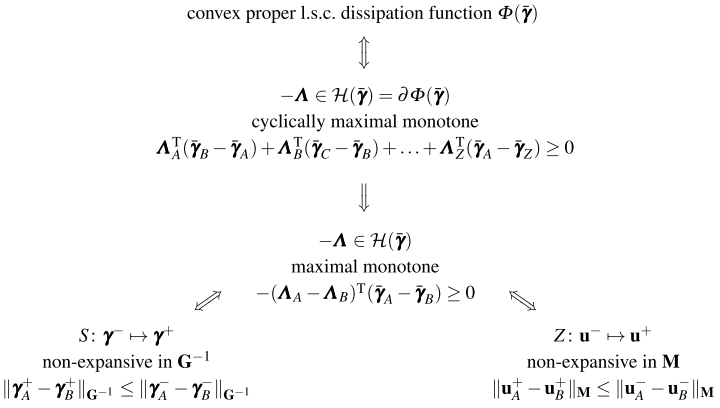

Fig. 2 Interrelations of a maximal monotone impact law [13]

Definition 1 (Maximal monotonicity [19]) A mapping $\mathcal{T}\colon \mathbb{R}^n \rightrightarrows \mathbb{R}^n$ is called monotone if it has the property that

$$(\mathbf{y}_A - \mathbf{y}_B)^{\mathrm{T}}(\mathbf{x}_A - \mathbf{x}_B) \geq 0 \tag{15}$$

whenever $\mathbf{y}_A \in \mathcal{T}(\mathbf{x}_A),\ \mathbf{y}_B \in \mathcal{T}(\mathbf{x}_B)$. Moreover, $\mathcal{T}$ is called maximal monotone if it is monotone and its graph cannot be enlarged without destroying this property.

Definition 2 (Nonexpansivity [13, 19]) A mapping $\mathcal{F}\colon \mathbb{R}^n \rightrightarrows \mathbb{R}^n$ is called nonexpansive in the metric induced by $\mathbf{P}$ if it has the property that

$$\|\mathbf{y}_A - \mathbf{y}_B\|_{\mathbf{P}} \leq \|\mathbf{x}_A - \mathbf{x}_B\|_{\mathbf{P}} \tag{16}$$

whenever $\mathbf{y}_A \in \mathcal{F}(\mathbf{x}_A),\ \mathbf{y}_B \in \mathcal{F}(\mathbf{x}_B)$.

Furthermore, the set-valued operator $\mathcal{H}$ can be written as the subdifferential to a convex proper lower semicontinuous (l.s.c.) dissipation function Φ such that

$$-\boldsymbol{\Lambda} \in \mathcal{H}(\bar{\boldsymbol{\gamma}}) = \partial\Phi(\bar{\boldsymbol{\gamma}}) \tag{17}$$

if and only if $\mathcal{H}$ is maximal cyclically monotone.

Definition 3 (Cyclical monotonicity [19]) A mapping $\mathcal{T}\colon \mathbb{R}^n \rightrightarrows \mathbb{R}^n$ is cyclically monotone if for any cycle of m points $\mathbf{x}_A, \mathbf{x}_B, \ldots, \mathbf{x}_Z$ (for arbitrary $m \geq 2$) and elements $\mathbf{y}_i \in \mathcal{T}(\mathbf{x}_i)$, we have

$$\mathbf{y}_A^{\mathrm{T}}(\mathbf{x}_B - \mathbf{x}_A) + \mathbf{y}_B^{\mathrm{T}}(\mathbf{x}_C - \mathbf{x}_B) + \cdots + \mathbf{y}_Z^{\mathrm{T}}(\mathbf{x}_A - \mathbf{x}_Z) \leq 0. \tag{18}$$

It is maximal cyclically monotone if it is cyclically monotone and its graph cannot be enlarged without destroying this property.

Note that cyclical monotonicity is a stronger condition than monotonicity. Definition 3 reduces to Definition 1 when $m = 2$. The relations between the nonexpansivity and monotonicity properties are shown in Fig. 2.

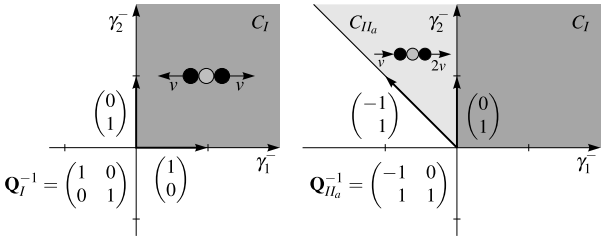

(a) Cone C_I (b) Cone C_{II_a}

Fig. 3 Construction steps of the impact mapping S

3 The sequential impact law

We propose a continuous conewise linear impact mapping $S\colon \mathbb{R}^2 \to \mathbb{R}^2,\ \boldsymbol{\gamma}^- \mapsto \boldsymbol{\gamma}^+$ for the 3-ball Newton's cradle. The impact mapping S takes the form

$$\boldsymbol{\gamma}^+ = S(\boldsymbol{\gamma}^-) = \mathbf{Q}_i \boldsymbol{\gamma}^- \quad \text{for } \boldsymbol{\gamma}^- \in C_i, \tag{19}$$

where the 2-by-2 matrices $\mathbf{Q}_i \in \mathbb{R}^{2\times 2}$ apply in a corresponding cone C_i in the (γ_1^-, γ_2^-)-plane. We construct the matrices $\mathbf{Q}_i$ together with their respective cones C_i by demanding the following properties of the impact law:

P1 The mapping is continuous, that is, $\mathbf{Q}_i \mathbf{v}_i = \mathbf{Q}_{i+1}\mathbf{v}_i$ with $\mathbf{v}_i$ being the direction of the boundary half-line between the adjacent cones C_i and C_{i+1}.

P2 Conservation of energy holds, that is, $\|\boldsymbol{\gamma}^+\|_{\mathbf{G}^{-1}} = \|\mathbf{Q}_i\boldsymbol{\gamma}^-\|_{\mathbf{G}^{-1}} = \|\boldsymbol{\gamma}^-\|_{\mathbf{G}^{-1}}$ for all matrices $\mathbf{Q}_i$. This implies energetic consistency.

P3 Each cone C_i is mapped by its matrix $\mathbf{Q}_i$ to the entire first quadrant, that is, the cone C_i is spanned by the columns of $\mathbf{Q}_i^{-1}$. This implies kinematic consistency.

We start with the first quadrant (see Fig. 3(a)). Preimpact contact velocities from the first quadrant are positive, which means that no impact occurs. Therefore, we set

$$\mathbf{Q}_I = \begin{pmatrix}1 & 0\\0 & 1\end{pmatrix}, \tag{20}$$

which means that $\boldsymbol{\gamma}^+ = \boldsymbol{\gamma}^-$ for all $\boldsymbol{\gamma}^- \in C_I$. The cone C_I is spanned by the columns of $\mathbf{Q}_I^{-1}$.

Next, we proceed to the cone C_{II_a} on the left of C_I as shown in Fig. 3(b). The boundary between the two cones is given by the positive γ_2^--axis. Continuity and conservation of energy (**P1** and **P2**) lead us to the matrix

$$\mathbf{Q}_{II_a} = \begin{pmatrix}-1 & 0\\1 & 1\end{pmatrix}. \tag{21}$$

The direction of the boundary to the next cone can be read from $\mathbf{Q}_{II_a}^{-1}$ (**P3**) as it is shown in Fig. 3(b), so that

$$\mathbf{v}_{II_a} = \begin{pmatrix}-1\\1\end{pmatrix}. \tag{22}$$

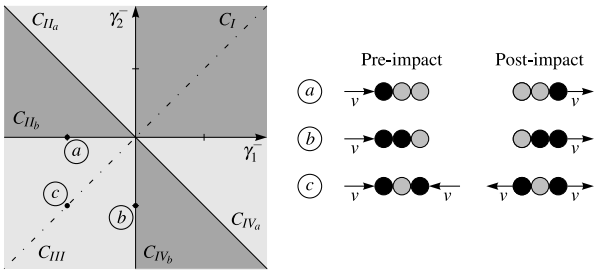

Fig. 4 *Left:* The different cones in the (γ_1^-, γ_2^-)-plane. The dot-dashed line marks the symmetry line. *Right:* Idealized observations

We can proceed analogously to find all six cones C_i with $i \in \{I, II_a, II_b, III, IV_a, IV_b\}$ together with their corresponding matrices

$$\begin{aligned} \mathbf{Q}_I &= \begin{pmatrix} 1 & 0 \\ 0 & 1 \end{pmatrix}, \qquad \mathbf{Q}_{II_a} = \begin{pmatrix} -1 & 0 \\ 1 & 1 \end{pmatrix}, \qquad \mathbf{Q}_{II_b} = \begin{pmatrix} 0 & 1 \\ -1 & -1 \end{pmatrix}, \\ \mathbf{Q}_{III} &= \begin{pmatrix} 0 & -1 \\ -1 & 0 \end{pmatrix}, \qquad \mathbf{Q}_{IV_a} = \begin{pmatrix} 1 & 1 \\ 0 & -1 \end{pmatrix}, \qquad \mathbf{Q}_{IV_b} = \begin{pmatrix} -1 & -1 \\ 1 & 0 \end{pmatrix}. \end{aligned} \tag{23}$$

The repartition of the (γ_1^-, γ_2^-)-plane into the six cones C_i with $i \in \{I, II_a, II_b, III, IV_a, IV_b\}$ is depicted in Fig. 4(a). The symmetry of the problem appears in the symmetry between the matrices $\mathbf{Q}_{II_a}$ and $\mathbf{Q}_{IV_a}$ and between $\mathbf{Q}_{II_b}$ and $\mathbf{Q}_{IV_b}$.

In the following, we will call the impact law (19) the *sequential impact law* because it is equivalent to a sequence of impacts between only two balls. This can be seen by the following properties:

$$\begin{aligned} \mathbf{Q}_{II_b} &= \mathbf{Q}_{IV_a}\mathbf{Q}_{II_a}, \\ \mathbf{Q}_{IV_b} &= \mathbf{Q}_{II_a}\mathbf{Q}_{IV_a}, \\ \mathbf{Q}_{III} &= \mathbf{Q}_{IV_a}\mathbf{Q}_{II_a}\mathbf{Q}_{IV_a} = \mathbf{Q}_{II_a}\mathbf{Q}_{IV_a}\mathbf{Q}_{II_a}, \end{aligned} \tag{24}$$

where $\mathbf{Q}_{II_a}$ and $\mathbf{Q}_{IV_a}$ describe the impact between only two of the three balls as will be shown below.

After having derived the sequential impact law, we want to argue why it is a reasonable choice. In the following, the implications of the sequential impact law are discussed for the four quadrants of the (γ_1^-, γ_2^-)-plane.

The first quadrant is equal to the cone C_I and corresponds to two positive preimpact contact velocities such that no impact happens. The identity map is the only reasonable choice for the first quadrant.

The third quadrant is equal to the cone C_{III} and corresponds to both preimpact contact velocities being negative and therefore kinematically admissible. Hence, the third quadrant contains all the classical experimental outcomes that can be realized with a 3-ball Newton's cradle. Figure 4(b) gives three examples of idealized observations from cone C_{III}. The sequential impact law provides these idealized experimental outcomes.

The second and fourth quadrants correspond to one preimpact contact velocity being positive and the other being negative. Each one of these quadrants contains two different cones because the magnitude of the positive preimpact contact velocity determines whether the corresponding outer ball participates in the impact process or not. The cones C_{II_a} and C_{IV_a}, which are adjacent to the first quadrant, correspond to a single impact between only two

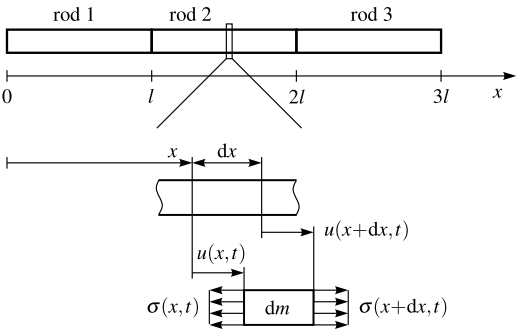

Fig. 5 Collision of three identical thin rods. The lower part shows the stresses acting on a differential element of the rod

of the three balls. In the cone C_{II_a}, the right ball does not participate in the impact process because it has a positive preimpact contact velocity that prevents it from colliding with the middle ball. This can be seen by considering the impact equation in the contact velocities (3) and the sequential impact law (19) for preimpact velocities $\boldsymbol{\gamma}^- \in C_{II_a}$,

$$\boldsymbol{\gamma}^+ - \boldsymbol{\gamma}^- = (\mathbf{Q}_{II_a} - \mathbf{I})\boldsymbol{\gamma}^- = \mathbf{G}\boldsymbol{\Lambda}, \tag{25}$$

where $\mathbf{I}$ denotes the identity matrix. Equation (25) yields the impulsive force

$$\boldsymbol{\Lambda} = \begin{pmatrix} -m\gamma_1^- \\ 0 \end{pmatrix}, \tag{26}$$

from which it becomes apparent that the right ball does not participate in the impact process. In C_{IV_a}, it is the left ball that is not subjected to any impact. For preimpact velocities belonging to the cones C_{II_a} and C_{IV_a}, the sequential impact law provides the same result as it is given by the generalized Newton's and generalized Poisson's impact laws for the nondissipative impact of two balls [7, 8]. The positive preimpact contact velocity in the cones C_{II_b} and C_{IV_b} does not prevent the interaction between the three balls through wave effects.

The third quadrant basically completely describes the physics of Newton's cradle as it covers all physically realizable experiments with Newton's cradle. Nevertheless, the first, the second, and the fourth quadrants are needed to deal with kinematically inadmissible preimpact contact velocities, which is important in view of numerical simulation. Small numerical errors may lead to positive preimpact contact velocities, and an impact law should map these preimpact contact velocities to physically reasonable postimpact contact velocities.

In the next section, we provide a further argument for the validity of the sequential impact law by showing that it provides the same outcomes as the one-dimensional wave equation does for the collision of three identical thin rods.

4 Thin rod model of the 3-ball Newton's cradle

Wave effects play a crucial role in the impact process of the 3-ball Newton's cradle. We model the system with three identical thin rods (see Fig. 5). This leads us to a description of the impact process that is governed by the one-dimensional wave equation.

The rods have cross-section A and density ρ. We consider the stresses acting on a differential element of the rod as it is shown in Fig. 5. The position of the differential element is

denoted by x. The displacement field is referred to as $u(x,t)$. The balance of linear momentum in x direction for the differential element is then given by

$$\mathrm{d}m\, u_{tt}(x,t) = A\big(\sigma(x+\mathrm{d}x,t) - \sigma(x,t)\big). \tag{27}$$

The mass element $\mathrm{d}m$ can be expressed in terms of $\mathrm{d}x$ as

$$\mathrm{d}m = \rho A \mathrm{d}x. \tag{28}$$

Further, we assume that the rods behave linear-elastically and thus obey Hooke's law

$$\sigma = E\varepsilon = E u_x, \tag{29}$$

where E and ε designate the Young's modulus and the strain, respectively. Using (28) and (29), we can rewrite (27) as

$$\rho A \mathrm{d}x\, u_{tt}(x,t) = AE\big(u_x(x+\mathrm{d}x,t) - u_x(x,t)\big). \tag{30}$$

Dividing (30) by $\rho A \mathrm{d}x$ and letting $\mathrm{d}x \to 0$ yield the classical one-dimensional wave equation

$$u_{tt}(x,t) = c^2 u_{xx}(x,t) \quad \text{with } c^2 = \frac{E}{\rho}, \tag{31}$$

where c denotes the propagation velocity of longitudinal waves in the rod.

Our aim is to investigate the impact effects in Newton's cradle by considering colliding rods. An impact between two colliding rods leads to discontinuities in the velocity and in the strain, which expand through the colliding rods with velocity c. These discontinuities can only propagate along characteristics of the solution of the wave equation (31). The construction of a characteristics diagram provides a way to investigate the wave propagation process. Detailed information about waves in elastic solids can be found in [10, 23]. In order to be able to construct characteristics diagrams, we first summarize some transition conditions of the longitudinal waves in Table 1.

4.1 Collision of two identical thin rods

We consider the collision of two identical thin rods. Before the impact, both rods are undeformed. Initially, the left rod has a uniform velocity v, and the right rod is at rest. We assume that the colliding ends of the rods have the same velocity as soon as they touch. The preimpact configuration can be seen in Fig. 6(a). The initial conditions can be stated as

$$\begin{aligned} u_x(x,0) &= 0 \quad \text{if } x \in [0,2l], \\ u_t(x,0) &= \begin{cases} v & \text{if } x \in [0,l], \\ 0 & \text{if } x \in (l,2l]. \end{cases} \end{aligned} \tag{32}$$

Discontinuities in the velocity and in the strain can only propagate along their characteristics. These characteristics of the wave equation (31) delimit regions of constant strain and velocity. Therefore, we state the strain and velocity for each region in the characteristics diagram in Fig. 6(a). The transition properties from Table 1 allow the construction of

Table 1 Transition properties of longitudinal waves in thin rods

Type	Diagram	Transition conditions
Free end	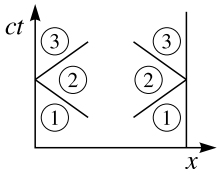	$u_{1,x} = 0$ $u_{3,x} = 0$ $u_{1,t} + u_{3,t} = 2u_{2,t}$
Impact between ends	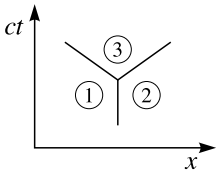	$u_{3,x} = \frac{1}{2c}(u_{2,t} - u_{1,t})$ $u_{3,t} = \frac{1}{2}(u_{2,t} + u_{1,t})$
Crossing waves	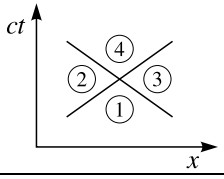	$u_{1,x} + u_{4,x} = u_{2,x} + u_{3,x}$ $u_{1,t} + u_{4,t} = u_{2,t} + u_{3,t}$

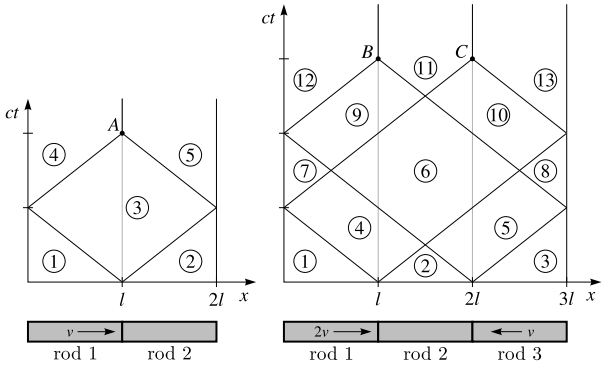

(a) Two rods (b) Three rods

Fig. 6 Characteristics diagrams for colliding identical thin rods

the characteristics diagram and the calculation of the corresponding strains and velocities, which are prevalent in the different regions in the characteristics diagram

$$\begin{aligned}
&\text{Region } ①\text{:} && u_{1,x} = 0, && u_{1,t} = v,\\
&\text{Region } ②\text{:} && u_{2,x} = 0, && u_{2,t} = 0,\\
&\text{Region } ③\text{:} && u_{3,x} = -\frac{v}{2c}, && u_{3,t} = \frac{v}{2},\\
&\text{Region } ④\text{:} && u_{4,x} = 0, && u_{4,t} = 0,\\
&\text{Region } ⑤\text{:} && u_{5,x} = 0, && u_{5,t} = v.
\end{aligned} \tag{33}$$

In A, the contact opens, the left rod is at rest, and the right rod has the uniform velocity v.

We can conclude that the collision of two identical thin rods leads to the same result as Newton's and Poisson's impact laws do for two balls in the nondissipative case. Moreover, the sequential impact law also provides this outcome in the cones C_{II_a} and C_{IV_a}, which correspond to the present situation of a single impact between two balls.

4.2 Collision of three identical thin rods

We now consider three identical thin rods. Initially, the middle rod is at rest. It is approached by the left and by the right rod, which have velocities $2v$ and $-v$, respectively. Again, the rods are undeformed before the collision. The initial conditions can be written as

$$u_x(x,0) = 0 \quad \text{if } x \in [0,3l],$$
$$u_t(x,0) = \begin{cases} 2v & \text{if } x \in [0,l], \\ 0 & \text{if } x \in (l,2l], \\ -v & \text{if } x \in (2l,3l]. \end{cases} \tag{34}$$

As in the previous case, we assume that the colliding ends of the rods have the same velocity as soon as they touch. Again, a characteristics diagram is constructed (see Fig. 6(b)) using the transition properties from Table 1. The following velocities and strains are obtained for the different regions ① to ⑬ in the characteristics diagram

$$\begin{aligned}
&\text{Reg. ①: } u_{1,x} = 0, && u_{1,t} = 2v, && \text{Reg. ⑧: } u_{8,x} = 0, && u_{8,t} = 0,\\
&\text{Reg. ②: } u_{2,x} = 0, && u_{2,t} = 0, && \text{Reg. ⑨: } u_{9,x} = -\frac{v}{2c}, && u_{9,t} = -\frac{v}{2},\\
&\text{Reg. ③: } u_{3,x} = 0, && u_{3,t} = -v, && \text{Reg. ⑩: } u_{10,x} = -\frac{v}{c}, && u_{10,t} = v,\\
&\text{Reg. ④: } u_{4,x} = -\frac{v}{c}, && u_{4,t} = v, && \text{Reg. ⑪: } u_{11,x} = 0, && u_{11,t} = 0,\\
&\text{Reg. ⑤: } u_{5,x} = -\frac{v}{2c}, && u_{5,t} = -\frac{v}{2}, && \text{Reg. ⑫: } u_{12,x} = 0, && u_{12,t} = -v,\\
&\text{Reg. ⑥: } u_{6,x} = -\frac{3v}{2c}, && u_{6,t} = \frac{v}{2}, && \text{Reg. ⑬: } u_{13,x} = 0, && u_{13,t} = 2v.\\
&\text{Reg. ⑦: } u_{7,x} = 0, && u_{7,t} = 0,
\end{aligned} \tag{35}$$

In B and C, both contacts open simultaneously. The left rod has a postimpact velocity of $-v$. The middle rod is at rest, and the right rod has a postimpact velocity of $2v$. This corresponds exactly to the outcome that is provided by the sequential impact law as can be seen by calculating the pre- and postimpact relative velocities of the rods

$$\boldsymbol{\gamma}^- = \begin{pmatrix} -2v \\ -v \end{pmatrix} \quad \text{and} \quad \boldsymbol{\gamma}^+ = \begin{pmatrix} v \\ 2v \end{pmatrix}, \tag{36}$$

for which indeed $\boldsymbol{\gamma}^+ = S(\boldsymbol{\gamma}^-) = \mathbf{Q}_{III}\boldsymbol{\gamma}^-$. Note that Newton's and Poisson's instantaneous impact laws would give a different outcome.

5 Compliant impact models

Considering compliant contacts is an alternative to instantaneous impact laws when modeling impacts between rigid bodies. In contrast to instantaneous impacts, the impact process is not reduced to a single time instant any more, but it extends to a finite time interval.

For colliding balls, the Hertz stiffness model [11] is often chosen to model the relationship between the contact force and the small contact penetration. The usually high contact stiffness results in stiff differential equations. The resulting numerical difficulties of the Hetz stiffness model or, more generally, a penalty approach, can be avoided by using the normal impulse as a time-like variable. Due to the nonnegativity of the contact force, the normal impulse increases monotonically with time. Therefore, the normal impulse can be used as an integration variable instead of time. Because of the high contact stiffnesses, the duration of the impact process is short compared to the characteristic time of the impact-free dynamics. Therefore, the position can be assumed to remain constant over the duration of the impact. Moreover, all forces other than the contact forces are neglected during the collision. This yields the Darboux–Keller approach [5, 12]. An extended Darboux–Keller approach, which can model multiple impacts, is presented in [15]. Energy losses at the contacts are considered by relating the work a respective normal contact force does during the expansion phase to the work it has done during the compression phase by using Stronge's energetic coefficient of restitution [21].

For the example of a dissipation-free chain of three equal balls considered in this paper, the extended Darboux–Keller approach from [15, 17] is equivalent to a compliant contact model [16]. With this modeling approach, the ratio between the contact stiffnesses influences the wave transmission behavior. For the 3-ball Newton's cradle, one would choose identical contact stiffnesses because of the symmetry of the system consisting of a chain of three identical steel balls. The 3-ball Newton's cradle should provide symmetric outcomes for symmetric initial conditions. If, for example, the initial condition $\mathbf{u}_1^- = (v\ 0\ 0)^\mathrm{T}$ with $v > 0$ results in the generalized postimpact velocity $\mathbf{u}_1^+ = (0\ 0\ v)^\mathrm{T}$, then the symmetric initial condition $\mathbf{u}_2^- = (0\,0\,-v)^\mathrm{T}$ should yield the generalized postimpact velocity $\mathbf{u}_2^+ = (-v\,0\,0)^\mathrm{T}$. This symmetry is only preserved if equal contact stiffnesses are chosen.

Nevertheless, it is interesting to consider contacts with unequal linear stiffnesses as it has been done in [1, 4, 16, Appendix C]. Again, we consider the situation where the left ball has velocity v and hits the middle and right balls that are standing still. If the stiffness of the left contact is much higher than the stiffness of the right one, then the outcome approaches the one prescribed by the sequential impact law (19). In the opposite situation where the stiffness of the left contact is much lower than the stiffness of the right one, the outcome of the compliant model approaches the solution provided by the generalized Newton's and Poisson's laws. The ratio of the contact stiffnesses determines how the kinetic energy is distributed among the three balls. The limiting cases of minimal and of maximal wave effects are given by Newton's/Poisson's law and by the sequential impact law, respectively. The mathematical properties of the sequential impact law for the 3-ball Newton's cradle are of interest because the Newton's cradle can be seen as a device in which the collision of three bodies of equal mass is associated with maximal wave effects compared to all imaginable experiments with three arbitrary bodies of equal mass [9].

We want to emphasize that the aim of this work is to investigate the mathematical structure of instantaneous impact laws. The question which modeling approach shows the best accordance with a certain set of experimental data remains untreated here. The readers interested in impact experiments are referred to [18, 20] and references therein.

6 Contraction properties of the sequential impact law

Since we are interested in the mathematical structure of impact laws, we investigate which properties from Fig. 2 hold for the sequential impact law.

6.1 Nonexpansivity of the sequential impact law

In the following, we show that the impact mapping (19) of the sequential impact law is nonexpansive in the metric induced by $\mathbf{G}^{-1}$. This means that the set-valued relationship (5) between the dual variables $\bar{\boldsymbol{\gamma}}$ and $\boldsymbol{\Lambda}$ is maximal monotone.

Theorem 1 *The impact mapping* (19) *is nonexpansive in the metric induced by* $\mathbf{G}^{-1}$, *that is*,

$$\left\|\boldsymbol{\gamma}_A^+ - \boldsymbol{\gamma}_B^+\right\|_{\mathbf{G}^{-1}} \leq \left\|\boldsymbol{\gamma}_A^- - \boldsymbol{\gamma}_B^-\right\|_{\mathbf{G}^{-1}} \quad \forall \boldsymbol{\gamma}_A^-, \boldsymbol{\gamma}_B^- \in \mathbb{R}^2. \tag{37}$$

Proof Condition (37) needs to hold for arbitrary pairs of preimpact contact velocities $\boldsymbol{\gamma}_A^-$ and $\boldsymbol{\gamma}_B^-$. The idea behind the proof is to decompose the line segment that connects the points $\boldsymbol{\gamma}_A^-$ and $\boldsymbol{\gamma}_B^-$ into a series of line segments that lie in a single cone. This decomposition can be done using a telescopic expansion

$$\left\|\boldsymbol{\gamma}_A^+ - \boldsymbol{\gamma}_B^+\right\|_{\mathbf{G}^{-1}} = \left\|\boldsymbol{\gamma}_A^+ - \boldsymbol{\gamma}_{*1}^+ + \boldsymbol{\gamma}_{*1}^+ - \boldsymbol{\gamma}_{*2}^+ + \cdots + \boldsymbol{\gamma}_{*k}^+ - \boldsymbol{\gamma}_B^+\right\|_{\mathbf{G}^{-1}}, \tag{38}$$

where the $\boldsymbol{\gamma}_{*i}^+$ are the images of $\boldsymbol{\gamma}_{*i}^-$ that lie on the boundaries between the cones. Figure 7(a) shows an example of this decomposition. At the boundary between the cones C_i and C_{i+1}, we have that $\boldsymbol{\gamma}_{*i}^+ = \mathbf{Q}_i \boldsymbol{\gamma}_{*i}^- = \mathbf{Q}_{i+1} \boldsymbol{\gamma}_{*i}^-$ due to continuity (**P1**). Therefore, Eq. (38) can be written as

$$\left\|\boldsymbol{\gamma}_A^+ - \boldsymbol{\gamma}_B^+\right\|_{\mathbf{G}^{-1}} = \left\|\mathbf{Q}_A\left(\boldsymbol{\gamma}_A^- - \boldsymbol{\gamma}_{*1}^-\right) + \mathbf{Q}_1\left(\boldsymbol{\gamma}_{*1}^- - \boldsymbol{\gamma}_{*2}^-\right) + \cdots + \mathbf{Q}_B\left(\boldsymbol{\gamma}_{*k}^- - \boldsymbol{\gamma}_B^-\right)\right\|_{\mathbf{G}^{-1}}. \tag{39}$$

From the triangle inequality it follows that

$$\begin{aligned}\left\|\boldsymbol{\gamma}_A^+ - \boldsymbol{\gamma}_B^+\right\|_{\mathbf{G}^{-1}} &= \left\|\mathbf{Q}_A\left(\boldsymbol{\gamma}_A^- - \boldsymbol{\gamma}_{*1}^-\right) + \mathbf{Q}_1\left(\boldsymbol{\gamma}_{*1}^- - \boldsymbol{\gamma}_{*2}^-\right) + \cdots + \mathbf{Q}_B\left(\boldsymbol{\gamma}_{*k}^- - \boldsymbol{\gamma}_B^-\right)\right\|_{\mathbf{G}^{-1}} \\ &\leq \left\|\mathbf{Q}_A\left(\boldsymbol{\gamma}_A^- - \boldsymbol{\gamma}_{*1}^-\right)\right\|_{\mathbf{G}^{-1}} + \left\|\mathbf{Q}_1\left(\boldsymbol{\gamma}_{*1}^- - \boldsymbol{\gamma}_{*2}^-\right)\right\|_{\mathbf{G}^{-1}} \\ &\quad + \cdots + \left\|\mathbf{Q}_B\left(\boldsymbol{\gamma}_{*k}^- - \boldsymbol{\gamma}_B^-\right)\right\|_{\mathbf{G}^{-1}}.\end{aligned} \tag{40}$$

Due to the energy conservation property **P2**, we have $\|\mathbf{Q}_i \boldsymbol{\gamma}^-\|_{\mathbf{G}^{-1}} = \|\boldsymbol{\gamma}^-\|_{\mathbf{G}^{-1}}$. This leads to

$$\left\|\boldsymbol{\gamma}_A^+ - \boldsymbol{\gamma}_B^+\right\|_{\mathbf{G}^{-1}} \leq \left\|\boldsymbol{\gamma}_A^- - \boldsymbol{\gamma}_{*1}^-\right\|_{\mathbf{G}^{-1}} + \left\|\boldsymbol{\gamma}_{*1}^- - \boldsymbol{\gamma}_{*2}^-\right\|_{\mathbf{G}^{-1}} + \cdots + \left\|\boldsymbol{\gamma}_{*k}^- - \boldsymbol{\gamma}_B^-\right\|_{\mathbf{G}^{-1}}. \tag{41}$$

Each $\boldsymbol{\gamma}_{*i}^-$ can be expressed in terms of $\boldsymbol{\gamma}_A^-$ and $\boldsymbol{\gamma}_B^-$ as the convex combination

$$\boldsymbol{\gamma}_{*i}^- = \alpha_i \boldsymbol{\gamma}_A^- + (1 - \alpha_i)\boldsymbol{\gamma}_B^- \quad \text{with} \ \ \alpha_i \in [0, 1]. \tag{42}$$

Equation (42) allows us to rewrite the terms of the right-hand side of (41) in the following way:

$$\begin{aligned}\left\|\boldsymbol{\gamma}_A^- - \boldsymbol{\gamma}_{*1}^-\right\|_{\mathbf{G}^{-1}} &= (1 - \alpha_1)\left\|\boldsymbol{\gamma}_A^- - \boldsymbol{\gamma}_B^-\right\|_{\mathbf{G}^{-1}}, \\ \left\|\boldsymbol{\gamma}_{*1}^- - \boldsymbol{\gamma}_{*2}^-\right\|_{\mathbf{G}^{-1}} &= (\alpha_1 - \alpha_2)\left\|\boldsymbol{\gamma}_A^- - \boldsymbol{\gamma}_B^-\right\|_{\mathbf{G}^{-1}}, \\ &\vdots \\ \left\|\boldsymbol{\gamma}_{*k}^- - \boldsymbol{\gamma}_B^-\right\|_{\mathbf{G}^{-1}} &= \alpha_k\left\|\boldsymbol{\gamma}_{*k}^- - \boldsymbol{\gamma}_B^-\right\|_{\mathbf{G}^{-1}}.\end{aligned} \tag{43}$$

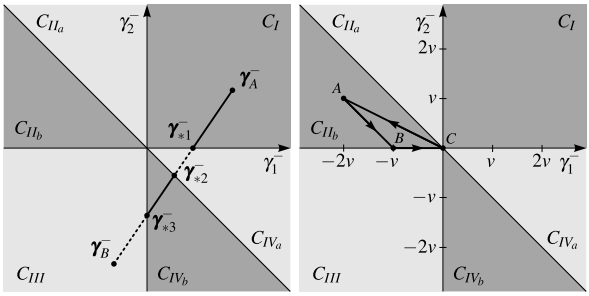

Fig. 7 *Left:* Exemplary decomposition of the path between $\boldsymbol{\gamma}_A^-$ and $\boldsymbol{\gamma}_B^-$. *Right:* ABC-cycle that provides a counterexample to the maximal cyclical monotonicity of the impact mapping S

Finally, we use the expressions from (43) to rewrite (41) as

$$\begin{aligned}\left\|\boldsymbol{\gamma}_A^+ - \boldsymbol{\gamma}_B^+\right\|_{\mathbf{G}^{-1}} \leq (1-\alpha_1)\left\|\boldsymbol{\gamma}_A^- - \boldsymbol{\gamma}_B^-\right\|_{\mathbf{G}^{-1}} + (\alpha_1-\alpha_2)\left\|\boldsymbol{\gamma}_A^- - \boldsymbol{\gamma}_B^-\right\|_{\mathbf{G}^{-1}} + \cdots \\ + \alpha_k\left\|\boldsymbol{\gamma}_{*k}^- - \boldsymbol{\gamma}_B^-\right\|_{\mathbf{G}^{-1}} \\ = \left\|\boldsymbol{\gamma}_A^- - \boldsymbol{\gamma}_B^-\right\|_{\mathbf{G}^{-1}}, \end{aligned} \tag{44}$$

which completes the proof. □

6.2 A counterexample to maximal cyclical monotonicity

In order to give a counterexample to the maximal cyclical monotonicity of (5) for the sequential impact law, we propose to consider an ABC-cycle that leads to a contradiction to inequality (18) in Definition 3. We consider the following ABC-cycle of preimpact contact velocities:

$$\boldsymbol{\gamma}_A^- = (-2v \quad v)^{\mathrm{T}}, \qquad \boldsymbol{\gamma}_B^- = (-v \quad 0)^{\mathrm{T}}, \qquad \boldsymbol{\gamma}_C^- = (0 \quad 0)^{\mathrm{T}}. \tag{45}$$

The cycle of preimpact contact velocities (45) is shown in Fig. 7(b). The sequential impact law (19) leads to the following postimpact contact velocities:

$$\boldsymbol{\gamma}_A^+ = (v \quad v)^{\mathrm{T}}, \qquad \boldsymbol{\gamma}_B^+ = (0 \quad v)^{\mathrm{T}}, \qquad \boldsymbol{\gamma}_C^+ = (0 \quad 0)^{\mathrm{T}}. \tag{46}$$

Using (6), (45), and (46), we obtain

$$\bar{\boldsymbol{\gamma}}_A = \left(-\tfrac{v}{2} \quad v\right)^{\mathrm{T}}, \qquad \bar{\boldsymbol{\gamma}}_B = \left(-\tfrac{v}{2} \quad \tfrac{v}{2}\right)^{\mathrm{T}}, \qquad \bar{\boldsymbol{\gamma}}_C = (0 \quad 0)^{\mathrm{T}}, \tag{47}$$

and from (3) the computation of the impulsive forces for the three impact cases follows:

$$\boldsymbol{\Lambda}_A = (2mv \quad mv)^{\mathrm{T}}, \qquad \boldsymbol{\Lambda}_B = (mv \quad mv)^{\mathrm{T}}, \qquad \boldsymbol{\Lambda}_C = (0 \quad 0)^{\mathrm{T}}. \tag{48}$$

Equations (47) and (48) allow the evaluation of inequality (18) from Definition 3 for the ABC-cycle

$$\boldsymbol{\Lambda}_A^{\mathrm{T}}(\bar{\boldsymbol{\gamma}}_B - \bar{\boldsymbol{\gamma}}_A) + \boldsymbol{\Lambda}_B^{\mathrm{T}}(\bar{\boldsymbol{\gamma}}_C - \bar{\boldsymbol{\gamma}}_B) + \boldsymbol{\Lambda}_C^{\mathrm{T}}(\bar{\boldsymbol{\gamma}}_A - \bar{\boldsymbol{\gamma}}_C) = \frac{-mv^2}{2} \leq 0. \tag{49}$$

Bearing in mind the minus sign from (5), we recognize that (49) is a contradiction to condition (18) from Definition 3. Thus, we can conclude that the set-valued operator $\mathcal{H}$ in (5) is not maximal cyclically monotone for the sequential impact law. Therefore, the sequential impact law cannot be expressed by a convex proper lower semicontinuous dissipation function $\Phi(\bar{\boldsymbol{\gamma}})$.

7 Conclusions

With the sequential impact law, an instantaneous impact law for completely elastic multicollisions of the 3-ball Newton's cradle has been formulated, which describes all idealized observations caused by wave-like phenomena. Moreover, the sequential impact law is in accordance with the postimpact velocities provided by the one-dimensional wave equation for the collision of three identical thin rods. The sequential impact law is kinematically, kinetically, and energetically consistent and has an impact mapping, which is continuous and conewise linear. It is shown in this paper that the impact mapping S of the sequential impact law is nonexpansive in the metric induced by the inverse Delassus matrix. Accordingly, the corresponding set-valued operator $\mathcal{H}$ between the impulsive force $\boldsymbol{\Lambda}$ and $\bar{\boldsymbol{\gamma}}$ is maximal monotone. Maximal monotonicity is a useful property to construct synchronization-based state observers for impacting systems [3]. The provided counterexample to maximal cyclical monotonicity allows us to conclude that no dissipation function exists for the sequential impact law.

The long-term goal is to develop an instantaneous impact law for completely elastic multicollisions of general multibody systems. The results on the 3-ball Newton's cradle may serve as a stepping stone to such a general impact law for completely elastic multicollisions and, finally, to also include dissipation. However, the question remains how the sequential impact law can be generalized to higher dimensions. A dissipation function would have provided such a generalization, but the current paper shows that a corresponding dissipation function does not exist. Future research will investigate other ways to arrive at a generalization.

Acknowledgements This research is supported by the Fonds National de la Recherche, Luxembourg (Proj. Ref. 8864427).

References

1. Acary, V., Brogliato, B.: Concurrent multiple impacts modelling: case-study of a 3-ball chain. In: Computational Fluid and Solid Mechanics, Second MIT Conference. Elsevier, Amsterdam (2003)
2. Acary, V., Brogliato, B.: Numerical Methods for Nonsmooth Dynamical Systems. Applications in Mechanics and Electronics. Lecture Notes in Applied and Computational Mechanics, vol. 35. Springer, Berlin (2008)
3. Baumann, M., Leine, R.I.: Convergence based synchronisation of unilaterally constrained multibody systems. In: Proceedings of the ENOC 2014 Conference, Vienna (2014)
4. Brogliato, B.: Nonsmooth Mechanics: Models, Dynamics and Control, 3rd edn. Springer, Berlin (2016)
5. Darboux, G.: Étude géométrique sur les percussions et les chocs des corps. Bul. Sci. Math. Astron., Deux. Sér. **4**(1), 126–160 (1880)
6. Glocker, Ch.: An introduction to impacts. In: Nonsmooth Mechanics of Solids. CISM Courses and Lectures, vol. 485, pp. 45–101. Springer, Vienna (2006)
7. Glocker, Ch.: Energetic consistency conditions for standard impacts, Part I: Newton-type inequality impact laws and Kane's example. Multibody Syst. Dyn. **29**(1), 77–117 (2013)
8. Glocker, Ch.: Energetic consistency conditions for standard impacts, Part II: Poisson-type inequality impact laws. Multibody Syst. Dyn. **32**(4), 445–509 (2014)

9. Glocker, Ch., Aeberhard, U.: The geometry of Newton's cradle. In: Alart, P., Maisonneuve, O., Rockafellar, R.T. (eds.) Nonsmooth Mechanics and Analysis. Theoretical and Numerical Advances, AMMA, vol. 12, pp. 185–194. Springer, Berlin (2006)
10. Graff, K.F.: Wave Motion in Elastic Solids. Clarendon Press, Oxford (1975)
11. Hertz, H.: Über die Berührung fester elastischer Körper. J. Reine Angew. Math. **92**, 156–171 (1882)
12. Keller, J.B.: Impact with friction. J. Appl. Mech. **53**, 1–4 (1986)
13. Leine, R.I., Baumann, M.: Variational analysis of inequality impact laws. In: Proceedings of the ENOC 2014 Conference, Vienna (2014)
14. Leine, R.I., van de Wouw, N.: Stability and Convergence of Mechanical Systems with Unilateral Constraints. Lecture Notes in Applied and Computational Mechanics, vol. 36. Springer, Berlin (2008)
15. Liu, C., Zhao, Z., Brogliato, B.: Frictionless multiple impacts in multibody systems. I. Theoretical framework. Proc. R. Soc. A **464**(2100), 3193–3211 (2008)
16. Nguyen, N.S., Brogliato, B.: Multiple Impacts in Dissipative Granular Chains. Lecture Notes in Applied and Computational Mechanics, vol. 72. Springer, Berlin (2014)
17. Nguyen, N.S., Zhang, H., Brogliato, B.: Multiple impacts with friction in the rocking block and tapered chains. In: Proceedings of the ENOC 2011 Conference, Rome (2011)
18. Payr, M.: An experimental and theoretical study of perfect multiple contact collisions in linear chains of bodies. Dissertation, ETH No. 17808, Zurich (2008)
19. Rockafellar, R.T., Wets, R.B.: Variational Analysis. Springer, Berlin (1998)
20. Seifried, R., Schiehlen, W., Eberhard, P.: The role of the coefficient of restitution on impact problems in multi-body dynamics. J. Multi-Body Dyn. **224**(3), 279–306 (2010)
21. Stronge, W.J.: Rigid body collisions with friction. Proc. R. Soc. Lond. A **431**(1881), 169–181 (1990)
22. Winandy, T., Leine, R.I.: Towards a maximal monotone impact law for Newton's cradle. In: Proceedings of the ECCOMAS Thematic Conference on Multibody Dynamics, Barcelona, Spain (2015)
23. Wittenburg, J.: Schwingungslehre. Springer, Berlin (1996)